We are IntechOpen, the world's leading publisher of Open Access books Built by scientists, for scientists

4,800
Open access books available

122,000
International authors and editors

135M
Downloads

Our authors are among the

154
Countries delivered to

TOP 1%
most cited scientists

12.2%
Contributors from top 500 universities

CLARIVATE ANALYTICS BOOK CITATION INDEX INDEXED

WEB OF SCIENCE™

Selection of our books indexed in the Book Citation Index in Web of Science™ Core Collection (BKCI)

Interested in publishing with us?
Contact book.department@intechopen.com

Numbers displayed above are based on latest data collected.
For more information visit www.intechopen.com

14

Computational Flow Modeling of Multiphase Mechanically Agitated Reactors

Panneerselvam Ranganathan[1] and Sivaraman Savithri[2]
[1]*Department of Geo Technology, Delft University of Technology, 2628 CN Delft,*
[2]*Computational Modeling & Simulation, National Institute for Interdisciplinary Science & Technology (CSIR), Thiruvananthapuram, Kerala,*
[1]*The Netherlands*
[2]*India*

1. Introduction

Mixing and dispersion of solids and gases in liquids in mechanically agitated reactors is involved in about 80% of the operations in the chemical industries, including processes ranging from leaching and complete dissolution of reagents to suspension of catalysts and reaction products, such as precipitates and crystals (Smith, 1990). This is one of the most widely used unit operations because of its ability to provide excellent mixing and contact between the phases.

An important aspect in the design of solids suspension in such reactors is the determination of the state of full particle suspension, at which point no particle remains in contact with the vessel bottom for more than 1 sec. Such a determination is critical because until such a condition is reached the total surface area of the particles is not efficiently utilized, and above this speed the rate of processes such as dissolution and ion exchange increases only slowly (Nienow, 1968).

Despite their widespread use, the design and operation of these agitated reactors remain a challenging problem because of the complexity encountered due to the three-dimensional (3D) circulating and turbulent multiphase flow in the reactor. Mechanically agitated reactors involving solid–liquid flows exhibit three suspension states: complete suspension, homogeneous suspension and incomplete suspension, as depicted in Figure 1 (Kraume, 1992).

A suspension is considered to be complete if no particle remains at rest at the bottom of the vessel for more than 1 or 2 sec. A homogeneous suspension is the state of solid suspension, where the local solid concentration is constant throughout the entire region of column. An incomplete suspension is the state, where the solids are deposited at the bottom of reactor. Hence, it is essential to determine the minimum impeller speed required for the state of complete off-bottom suspension of the solids, called the critical impeller speed. It is denoted by N_{js} for solid suspension in the absence of gas and by N_{jsg} for solid suspension in the presence of gas. A considerable amount of research work has been carried out to determine the critical impeller speed starting with the pioneering work of Zwietering (1958) who

Source: Computational Fluid Dynamics, Book edited by: Hyoung Woo OH,
ISBN 978-953-7619-59-6, pp. 420, January 2010, INTECH, Croatia, downloaded from SCIYO.COM

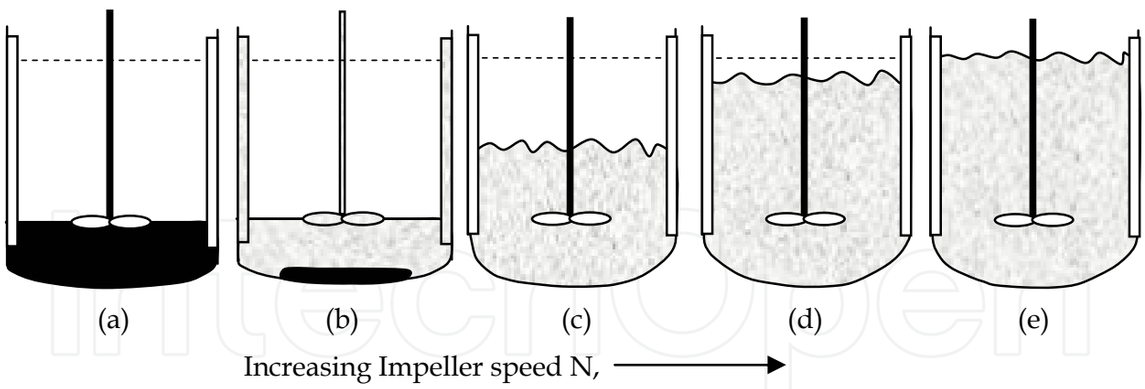

Fig. 1. Flow regimes of liquid–solid stirred reactor (Kraume, 1992)

proposed a correlation for the minimum impeller speed for complete suspension of solids on the basis of dimensional analysis of the results obtained from over a thousand experiments. Since then, numerous papers on determination of critical impeller speed for different operating conditions and different types of impellers have been published (Bohnet and Niesmak, 1980; Chapman et al., 1983a; Kraume, 1992) for liquid–solid stirred reactors, and a few of them (Zlokarnik & Judat, 1969; Chapman et al., 1983b; Warmoeskerken et al., 1984; Nienow et al., 1985; Bujalski et al., 1988; Wong et al., 1987; Frijlink et al., 1990; Rewatkar et al., 1991; Dylag & Talaga, 1994; Dutta & Pangarkar, 1995; Pantula & Ahmed, 1998; Zhu & Wu, 2002) have been extended towards the development of correlations for the critical impeller speed for gas–liquid–solid stirred reactors.

According to the literature, in general, N_{jsg} is always greater than N_{js}. Zlokarnik and Judat (1969) have reported that approximately 30% higher impeller speed over N_{js} is required to ensure the resuspension of solid, when gas is introduced. This is due to the reduction in impeller pumping capacity. The reason for the reduction in impeller power in three-phase agitated reactor system has been extensively studied in the literature. Chapman et al. (1983b) explained the decreased liquid pumping capacity and power input on the basis of the sedimentation phenomena. Warmoeskerken et al. (1984) explained the decrease in impeller power due to the formation of gas-filled cavities behind the impeller blades. Rewatkar et al. (1991) reported that the reduction in the impeller power in the three-phase system is due to the formation of solid fillet at the center and along the periphery of the vessel bottom and the formation of gas-filled cavities behind the impeller. Tables 1 & 2 show empirical correlations developed by various authors for the determination of critical impeller speed from their own experimental data for solid–liquid and gas–solid–liquid mechanically agitated reactors.

The critical impeller speed for liquid–solid and gas–liquid–solid mechanically agitated reactors depend on several parameters, such as particle settling velocity, impeller design, impeller diameters and sparger design, and its location. The selection of impeller type is an important consideration for simultaneous solid suspension and gas dispersion with minimum power requirement in such reactors. In the literature, various authors (Chapman et al., 1983b; Frijlink et al., 1990; Rewatkar et al., 1991; Pantula & Ahmed, 1998) have studied the performance of different types of impellers for a solid suspension in a stirred tank for various ranges of operating conditions and concluded that the pitched blade turbine with

downward pumping (PBTD) is more favorable at lower gassing rates and disc turbine (DT) and pitched blade turbine with upward pumping (PBTU) is more favorable at higher gassing rate.

Authors	Experimental system used	Empirical Correlation
Zweitering (1958)	Impeller type = Propeller, Disc and 2-paddle T = 0.154–1.0 m D = 0.06–0.26 m C = 0.051E-02–0.076E-02 m Particle density = 2500 kg /m^3 Dp = 125–850 µm Solid loading = 0.34–3.4 wt %	$N_{js} = \frac{S\gamma^{0.1} dp^{0.2} \left(\frac{g\Delta\rho}{\rho_l}\right)^{0.45}}{D^{0.85}} x^{0.13}$
Nienow (1968)	Impeller type = 6-DT T = 0.14m D = 0.0364, 0.049, 0.073 Dp =153–9000 µm Particle density =530–1660 kg/m^3 Solid loading = 0.1–1.0 wt %	$N_{js} = \frac{(\Delta\rho/\rho_l)^{0.43} dp^{0.21}}{D^{2.25}} x^{0.12}$
Narayanan et al. (1969)	Impeller type = 8-Paddle T = 0.114,0.141 m D = 0.036–0.057 m Particle density =140–1600 kg/m^3 Dp =106–600 µm Solid loading = 2.5–20 wt %	$N_{js} = \frac{0.9v}{2T - D}\left(\frac{T}{D}\right)^2$ $v = \sqrt{\left(2g\left(\rho_p - \rho_l\right)\left(\frac{2dp}{3\rho_p} + \frac{X_s H_{sl}}{\rho_p + H_{sl}\rho_l}\right)\right.}$
Raghava Rao et al. (1988)	Impeller type = 6-DT, 6-PTD, 6-PDU T= 0.3–0.15 m D = 0.175–0.58 m C = 0.5T– 0.167T W/D = 0.25–0.4 Particle density = 1520 kg/m^3 Solid loading = 0–50 wt % Dp =100–2000 µm	$N_{js} = \frac{f\gamma^{0.1}\left(\frac{g\Delta\rho}{\rho_l}\right)^{0.45} X^{0.1} dp^{0.11} T^{0.31}}{D^{1.16}}$
Takahashi et al. (1993)	T = 0.1–0.58 m Impeller type = 6-DT D = 0.05–0.29 m C = 0.0125-0.0725 m Dp = 50–5000 µm Particle density=1049–3720 kg/m^3 Solid concentration = 0.1–2 vol. %	$N_{js} \propto \frac{\mu^{0.1}\left(\frac{g\Delta\rho}{\rho_l}\right)^{0.34} X^{0.22} dp^{0.023}}{D^{0.54}}$ $N_{js} \propto \frac{\mu^{0.1}\left(\frac{g\Delta\rho}{\rho_l}\right)^{0.38} X^{0.17} dp^{0.05}}{D^{0.6}}$

Rieger and Ditl (1994)	Impeller type = pitched six blade turbines with 45° T= 0.2, 0.3, 0.4 m D= T/3 C = 0.5D Dp = 0.18–6 mm Particle density = 1243 kg/m^3 Solid concentration= 2.5, 10 vol. %	$N_{js} \propto (\Delta\rho/\rho_l)^{0.5} D^{-0.5}$ $N_{js} \propto (\Delta\rho/\rho_l)^{0.5} d_p^{0.3} D^{-0.8}$ $N_{js} \propto \Delta\rho^{0.42} \rho_l^{-0.58} \mu^{0.16} D^{-0.73}$ $N_{js} \propto \Delta\rho^{0.42} \rho_l^{-0.58} \mu^{0.16} d_p^{0.25} D^{-0.99}$
Ibrahim & Nienow (1996)	Impeller type = 6-DT, 6-FDT, 6-PDT T = 0.292,0.33 m D = 0.065–0.102 Particle density = 2500 kg/m^3 Dp = 110 µm Solid concentration = 0.5 vol %	$N_{js} = \frac{S\gamma^{0.1} dp^{0.2} \left(\frac{g\Delta\rho}{\rho_l}\right)^{0.45}}{D^{0.85}} x^{0.13}$
Armenante & Nagamine (1998)	Impeller type = 6-DT, 6-FBT, 6-PTD, HE-3 T= 0.188–0.584 m D= 0.0635–0.203m Particle density = 2500 kg/m^3 Dp =60–300 µm Solid concentration = 0.5 vol %	$N_{js} = \frac{S\gamma^{0.1} dp^{0.2} \left(\frac{g\Delta\rho}{\rho_l}\right)^{0.45}}{D^{0.13}} x^{0.13}$
Bujalski et al. (1999)	Impeller type = A310, A315 T= 0.29 m D= 0.10–0.12 m Particle density=1350–500kg/m^3 Dp = 100–1000 µm Solid concentration = 0–40%	$N_{js} = \frac{S\gamma^{0.1} dp^{0.2} \left(\frac{g\Delta\rho}{\rho_l}\right)^{0.45}}{D^{0.85}} x^{0.13}$
Sharma & Shaikh (2003)	Impeller type: 4,6-PTD T= 0.15–1.21 m D= 0.0535-0.348 m Particle density=1390–635kg/m^3 Dp = 130–850 µm Solid concentration =1.55–2 vol.%	$N_{js} = \frac{S\gamma^{0.1} dp^{0.2} \left(\frac{g\Delta\rho}{\rho_l}\right)^{0.45}}{D^{-2.0}} x^{0.13}$
Dohi et al. (2004)	Impeller type = Maxblend, PTD Fullzone,Pfaudler T= 0.2–0.8 m D= 0.42T–0.53T m Particle density = 2500 kg/m^3 Dp = 187–810 µm Solid concentration =0–30 by vol.%	$N_{js} = \frac{S\gamma^{0.1} dp^{0.2} \left(\frac{g\Delta\rho}{\rho_l}\right)^{0.45}}{D^{-0.85}} x^{0.13}$

Table 1. Empirical correlations for the critical impeller speed from the literature for solid–liquid mechanically agitated reactors

Another criterion which is also used for assessing the quality of solids suspension is the degree of homogeneity of suspension. Einenkel (1979), suggested the variance of solid concentration as a measure of homogeneity of the solids suspension, which is defined as

$$\sigma^2 = \frac{1}{n}\sum_{1}^{n}\left(\frac{C}{\overline{C}} - 1\right)^2 \quad (1)$$

References	Experimental system used	Empirical correlation
Chapman et al.(1983b)	tank diameter = 0.29–1.83 m, Impeller type = DT, PBTD and PBTU and marine propeller impeller clearance = T/4 solid loading = 0.34–50 wt % particle density = 1050– 2900 kg /m^3 particle diameter = 100–2800 µm air flow rate = 0–32 mm/s sparger type = ring, pipe, conical and concentric rings	$\Delta N_{js} = N_{jsg} - N_{js}$ $= kQ_v$ where k=0.94
Nienow et al.(1985)	tank diameter = 0.45 m impeller type = Disc turbine impeller diameter = 0.225 m impeller clearance = 0.1125 m particle type = glass beads particle diameter = 440–530 µm	$\Delta N_{js} = N_{jsg} - N_{js}$ $= kQ_v$ where k=0.94
Wong et al.(1987)	tank diameter = 0.29 m impeller type = Propeller, Disc and Pitched turbine impeller diameter = 0.06–0.26 m impeller clearance = 0.051– 0.076 m particle density = 2514–8642 kg /m^3 particle diameter = 200–1200 µm air flow rate = 0–2 vvm	$\Delta N_{js} = N_{jsg} - N_{js}$ $= kQ_v$ where k=2.03 for DT, k=4.95 for PBTD
Rewatkar et al.(1991)	tank diameter = 0.57–1.5 m, impeller type = RT, PBTD and PBTU impeller diameter = 0.175T–0.58T m impeller clearance = T/3 particle diameter = 100–2000 µm air flow rate = 0–32 mm/s Solid loading = 0.34–50 wt % sparger type = ring, pipe, conical and concentric rings	$\Delta N_s = 132.7 V_{s\infty}^{0.5} D^{-1.67} T V_g$ where $\Delta N_s = N_{jsg} - N_{sp}$ N_{sp}= critical impeller speed for solid suspension in the presence of sparger N_{jsg}= critical impeller speed for suspension in gas-liquid-solid system $V_{s\infty}$= terminal setting velocity of particle

Dylag and Talaga (1994)	tank diameter = 0.3 m and ellipsoidal bottom impeller type = DT and PBTD impeller clearance = 0.5D particle density = 2315 kg /m3 particle diameter = 0.248–0.945 mm air flow rate = 1.5–22.5 mm/s solid loading = 2–30 wt %	For DT $\frac{N_{jsg}D^2\rho_c}{\eta_c} = 18.95\times10^4\left(\frac{v_G D\rho_g}{\eta_g}\right)^{0.15}$ $\chi^{0.15}\left(\frac{d_p}{D}\right)^{0.20}$ For PBTD $\frac{N_{jsg}D^2\rho_c}{\eta_c} = 17.55\times10^4\left(\frac{v_G D\rho_g}{\eta_g}\right)^{0.31}$ $\chi^{0.15}\left(\frac{d_p}{D}\right)^{0.20}$

Table 2. Empirical correlations for the critical impeller speed from the literature for gas–solid– liquid mechanically agitated reactors

Bohnet and Niesmak (1980) used the square root of variance, which corresponds to the standard deviation of the concentration profile (σ). Kraume, (1992) used another measure to evaluate the homogeneity of suspension which is based on the cloud height. The suspension is said to be homogeneous when the solid concentration is uniform throughout the tank. When the slurry height or cloud height becomes equal to 0.9H, the state of suspension is said to be homogeneous where H refers to the height of the reactor. Even though the suspended slurry height or cloud height is not an absolute measure of homogeneity, it may be useful for comparing the identical slurries.

During the last few decades, various models have been proposed for quantifying the solid suspension from the theoretical power requirement. Kolar (1967) presented a model for solid suspension based on energy balance, that all the power is consumed for suspending the solids and that the stirred tank is hydrodynamically homogeneous. Baldi et al. (1978) proposed a new model for complete suspension of solids where it is assumed that the suspension of particles is due to turbulent eddies of certain critical scale. Further it is assumed that the critical turbulent eddies that cause the suspension of the particles being at rest on the tank bottom have a scale of the order of the particles size, and the energy transferred by these eddies to the particles is able to lift them at a height of the order of particle diameter. Since their hypothesis related to the energy dissipation rate for solid suspension to the average energy dissipation in the vessel by employing modified Reynolds number concept, it gave good insight into the suspension process compared to other approaches. Chudacek (1986) proposed an alternative model for the homogeneous suspension based on the equivalence of particle settling velocity and mean upward flow velocity at the critical zone of the tank which leads to the constant impeller tip speed criterion, but this is valid only under conditions of geometric and hydrodynamic similarity. Shamlou and Koutsakos (1989) introduced a theoretical model based on the fluid dynamics and the body force acting on solid particles at the state of incipient motion and subsequent suspension. Rieger and Ditl (1994) developed a dimensionless equation for the critical impeller speed required for complete suspension of solids based on the inspection analysis of governing fluid dynamic equations. They observed four different hydrodynamic regimes based on the relative particle size and Reynolds number values.

Although the available correlations in the literature are of great importance from an operational view-point, they do not provide a clear understanding of the physics underlying the system. From a physical standpoint, the state of suspension of solid particles in the reactor is completely governed by the hydrodynamics and turbulence prevailing in the reactor. Only a few studies (Guha et al., 2007; Spidla et al., 2005 (a,b); Aubin et al., 2004) have been made to understand the complex hydrodynamics of such complicated stirred reactors. Even though in the recent past, both invasive and non invasive experimental measurement techniques have been reported in the literature, a systematic experimental study to characterize the solid hydrodynamics in mechanically agitated reactors can hardly be found in the literature.

For this reason, computational fluid dynamics (CFD) has been promoted as a useful tool for understanding multiphase reactors (Dudukovic et al., 1999) for precise design and scale up. Although much experimental effort has been focused on developing correlations for just-suspension speed, CFD simulations offer the only cost-effective means to acquire the detailed information on flow and turbulence fields needed for realistic distributed-parameter process simulations. The RANS-based CFD approach is the most widely used approach for the multiphase phase flow simulation of such reactors. In the literature, CFD based simulations have been used to predict the critical impeller speed for a solid suspension in a liquid–solid stirred tank reactor (Bakker et al., 1994; Micale et al., 2000; Barrue et al., 2001; Sha et al., 2001; Kee and Tan, 2002; Montante & Magelli 2005; Khopkar et al., 2006; Guha et al., 2008) by employing the Eulerian–Eulerian approach, and this prediction have been extended to the case of gas–liquid–solid stirred tank reactors. Recently Murthy et al. (2007) carried out CFD simulations for three-phase stirred suspensions. The effect of tank diameter, impeller diameter, type, location, size, solid loading and superficial gas velocity on the critical impeller speed was investigated by them using the standard deviation approach. The solid loading in their study varied from 2–15% by weight. But most of the industrial applications, especially hydrometallurgical applications, involve high density particles with high concentration. Moreover, it has been reported in the literature (Khopkar et al., 2006; van der Westhuizen & Deglon, 2008) that it is difficult to quantify the critical impeller just based on the standard deviation approach alone.

Hence, the objective of this work is to carry out the CFD simulation based on the Eulerian multi-fluid approach for the prediction of the critical impeller speed for high density solid particles with solid loading in the range of 10–30% by weight. CFD Simulations were carried out using the commercial package ANSYS CFX-10. Since any CFD simulation has to be validated first, the CFD simulations have been validated with those reported in the literature (Guha et al., 2007; Spidla et al., 2005; Aubin et al., 2004) for solid–liquid agitated reactors. After the validation, the CFD simulations have been extended for gas–liquid–solid mechanically agitated contactor to study the effects of impeller design, impeller speed, particle size and gas flow rate on the prediction of critical impeller speed based on both the standard deviation approach and cloud height criteria, and the simulation results were compared with our experimental results.

2. CFD modeling

2.1 Eulerian multiphase model

Even though CFD models have shown to be successful in simulating single-phase flow generated by impeller(s) of any shape in complex reactors (Ranade, 2002), the complexity of

modeling increases considerably for multiphase flows because of various levels of interaction of different phases. Two widely used modeling methods for multiphase flows are Eulerian–Eulerian or two fluid approach and Eulerian–Lagrangian approach. In Eulerian–Lagrangian approach, trajectories of dispersed phase particles are simulated by solving an equation of motion for each dispersed phase particle. Motion of the continuous phase is modeled using a conventional Eulerian framework. Depending on the degree of coupling (one–way, two–way or four–way), solutions of both phases interact with each other. But this approach can only be used for multiphase systems with a low solid volume fraction (≤ 5%) because of the tremendous computational need. In Eulerian–Eulerian approach, the dispersed phase is treated as a continuum. All phases 'share' the domain and may interpenetrate as they move within it. This approach is more suitable for modeling dispersed multiphase systems with a significant volume fraction of dispersed phase (>10%). But the coupling between different phases is incorporated in this approach by developing suitable interphase transport models. The computational details along with merits and demerits of these two approaches are given in the book by Ranade (2002).

For the present work, the liquid–solid/gas–liquid–solid flows in mechanically agitated contactor are simulated using Eulerian multi-fluid approach. Each phase is treated as a different continuum which interacts with other phases everywhere in the computational domain. The share of the flow domain occupied by each phase is given by the volume fraction. Each phase has its own velocity, temperature and physical properties. In this work, both gas and solid phases are treated as dispersed phases and the liquid phase is treated as continuous. The motion of each phase is governed by respective Reynolds averaged mass and momentum conservation equations. The general governing equations are given below:

Continuity equation:

$$\frac{\partial}{\partial t}\left(\epsilon_k \rho_k\right) + \nabla.\left(\rho_k \epsilon_k \vec{u}_k\right) = 0 \tag{2}$$

where ρ_k is the density and ϵ_k is the volume fraction of phase k (liquid, gas or solid) and the volume fraction of the all phases satisfy the following condition:

$$\sum_k \epsilon_k = 1 \tag{3}$$

Momentum Equations:

$$\frac{\partial}{\partial t}.\left(\rho_k . \epsilon_k . \vec{u}_k\right) + \nabla.\left(\rho_k . \epsilon_k . \vec{u}_k \vec{u}_k\right) - \nabla.\left(\epsilon_k \mu_{eff,k}\left(\nabla \vec{u}_k + \left(\nabla \vec{u}_k\right)^T\right)\right) = -\epsilon_k . \nabla P + \rho_k . \epsilon_k . \vec{g} + F \tag{4}$$

where $\mu_{eff,k}$ is the phase viscosity, P is the pressure, g is the gravitational acceleration and F stands for time averaged interface force between different phases and are discussed in detail below.

Interphase transport models

There are various interaction forces such as the drag force, the lift force and the added mass force etc. during the momentum exchange between the different phases. But the main interaction force is due to the drag force caused by the slip between the different phases. Recently, Khopkar et al. (2003, 2005) studied the influence of different interphase forces and reported that the effect of the virtual mass force is not significant in the bulk region of

agitated reactors and the magnitude of the Basset force is also much smaller than that of the inter-phase drag force. Further they also reported that the turbulent dispersion terms are significant only in the impeller discharge stream. Very little influence of the virtual mass and lift force on the simulated solid holdup profiles was also reported by Ljungqvist and Rasmuson (2001). Hence based on their recommendations and also to reduce the computational time, the interphase drag force and turbulent dispersion force are considered in this work.

Solid-liquid mechanically agitated reactor

For this case, the liquid phase is treated as a continuous phase and the solid phase is treated as a dispersed phase. The corresponding momentum equations are
Liquid phase (continuous phase)

$$\frac{\partial}{\partial t}.\left(\rho_l.\in_l.\vec{u}_l\right)+\nabla.\left(\rho_l.\in_l.\vec{u}_l\vec{u}_l\right)=-\in_l.\nabla P+\nabla.\left(\in_l \mu_{eff,l}\left(\nabla\vec{u}_l+\left(\nabla\vec{u}_l\right)^T\right)\right)+\rho_l\in_l\vec{g}+\vec{F}_{D,ls}+\vec{F}_{TD} \quad (5)$$

Solid phase (dispersed solid phase)

$$\begin{aligned}&\frac{\partial}{\partial t}.\left(\rho_s.\in_s.\vec{u}_s\right)+\nabla.\left(\rho_s.\in_s.\vec{u}_s\vec{u}_s\right)=\\&-\in_s.\nabla P-\nabla P_s+\nabla.\left(\in_s \mu_{eff,s}\left(\nabla\vec{u}_s+\left(\nabla\vec{u}_s\right)^T\right)\right)+\rho_s.\in_s.\vec{g}-\vec{F}_{D,ls}-\vec{F}_{TD}\end{aligned} \quad (6)$$

where the interphase drag force between the liquid and solid phases is represented by the equation

$$\vec{F}_{D,ls}=C_{D,ls}\frac{3}{4}\rho_l\frac{\in_s}{d_p}\left|\vec{u}_s-\vec{u}_l\right|\left(\vec{u}_s-\vec{u}_l\right) \quad (7)$$

where the drag coefficient proposed by Brucato et al. (1998) is used viz.,

$$\frac{C_{D,ls}-C_{D0}}{C_{D0}}=8.67\times10^{-4}\left(\frac{d_p}{\lambda}\right)^3 \quad (8)$$

where, d_p is the particle size and λ is the Kolmogorov length scale, C_{D0} is the drag coefficient in stagnant liquid which is given as

$$C_{D0}=\frac{24}{Re_p}\left(1+0.15Re_p^{0.687}\right) \quad (9)$$

where Re_p is the particle Reynolds number.
The turbulent dispersion force is the result of the turbulent fluctuations of liquid velocity which approximates the diffusion of the dispersed phase from higher region to lower region. The following equation for the turbulent dispersion force derived by Lopez de Bertodano (1992) is used for the present simulation and is given by

$$\vec{F}_{TD}=-C_{TD}\rho_l k_l\nabla\in_l \quad (10)$$

where C_{TD} is a turbulent dispersion coefficient, and is taken as 0.1 for the present investigation.

Gas-liquid-solid mechanically agitated reactor

For this case, the liquid phase is treated as a continuous phase and both the gas and the solid phases are treated as dispersed phases. The interphase forces considered for this simulation are the drag forces between liquid and solid, and liquid and gas and the turbulent dispersion force. The corresponding momentum equations are
Gas phase (dispersed fluid phase)

$$\frac{\partial}{\partial t}.\left(\rho_g.\in_g.\vec{u}_g\right)+\nabla.\left(\rho_g.\in_g.\vec{u}_g\vec{u}_g\right)=-\in_g.\nabla P+\nabla.\left(\in_g \mu_{eff,g}\left[\nabla\vec{u}_g+\left(\nabla\vec{u}_g\right)^T\right]\right)+\rho_g.\in_g.\vec{g}-\vec{F}_{D,lg} \quad (11)$$

Liquid phase (continuous phase)

$$\begin{aligned}&\frac{\partial}{\partial t}.\left(\rho_l.\in_l.\vec{u}_l\right)+\nabla.\left(\rho_l.\in_l.\vec{u}_l\vec{u}_l\right)=\\&-\in_l.\nabla P+\nabla.\left(\in_l \mu_{eff,l}\left[\nabla\vec{u}_l+\left(\nabla\vec{u}_l\right)^T\right]\right)+\rho_l\in_l\vec{g}+\vec{F}_{D,lg}+\vec{F}_{D,ls}+\vec{F}_{TD}\end{aligned} \quad (12)$$

Solid phase (dispersed solid phase)

$$\begin{aligned}&\frac{\partial}{\partial t}.\left(\rho_s.\in_s.\vec{u}_s\right)+\nabla.\left(\rho_s.\in_s.\vec{u}_s\vec{u}_s\right)\\&=-\in_s.\nabla P-\nabla P_s+\nabla.\left(\in_s \mu_{eff,s}\left[\nabla\vec{u}_s+\left(\nabla\vec{u}_s\right)^T\right]\right)+\rho_s.\in_s.\vec{g}-\vec{F}_{D,ls}-\vec{F}_{TD}\end{aligned} \quad (13)$$

The drag force between the solid and liquid phases and the turbulent dispersion force are the same as given by equations (7–9). The drag force between the gas and liquid phases is represented by the equation

$$\vec{F}_{D,lg}=C_{D,lg}\frac{3}{4}\rho_l\frac{\in_g}{d_b}\left|\vec{u}_g-\vec{u}_l\right|\left(\vec{u}_g-\vec{u}_l\right) \quad (14)$$

where the drag coefficient exerted by the dispersed gas phase on the liquid phase is obtained by the modified Brucato drag model (Khopkar et al., 2003), which accounts for interphase drag by microscale turbulence and is given by

$$\frac{C_{D,lg}-C_D}{C_D}=6.5\times10^{-6}\left(\frac{d_p}{\lambda}\right)^3 \quad (15)$$

where C_D is the drag coefficient of single bubble in a stagnant liquid and is given by

$$C_D=\mathrm{Max}\left(\frac{24}{Re_b}\left(1+0.15Re_b^{0.687}\right),\frac{8}{3}\frac{Eo}{Eo+4}\right) \quad (16)$$

where Eo is Eotvos number, Re_b is the bubble Reynolds number and they are given by

$$Re_b=\frac{\left|\vec{u}_l-\vec{u}_g\right|d_b}{\nu_l} \quad (17)$$

$$Eo = \frac{g\left(\rho_l - \rho_g\right)d_b{}^2}{\sigma} \tag{18}$$

Closure law for turbulence

In the present study, the standard k-ε turbulence model for single phase flows has been extended for turbulence modeling of two/three phase flows in mechanically agitated contactors. The corresponding values of k and ε are obtained by solving the following transport equations for the turbulence kinetic energy and turbulence dissipation rate.

$$\frac{\partial\left(\in_l \rho_l k_l\right)}{\partial t} + \nabla.\left(\in_l \left(\rho_l \vec{u}_l k_l - \left(\mu + \frac{\mu_{tl}}{\sigma_k}\right)\Delta k_l\right)\right) = \in_l \left(P_l - \rho_l \varepsilon_l\right) \tag{19}$$

$$\frac{\partial\left(\in_l \rho_l \varepsilon_l\right)}{\partial t} + \nabla.\left(\in_l \rho_l \vec{u}_l k_l - \left(\mu + \frac{\mu_{tl}}{\sigma_\varepsilon}\right)\Delta \varepsilon_l\right) = \in_l \frac{\varepsilon_l}{k_l}\left(C_{\varepsilon 1} P_l - C_{\varepsilon 2}\rho_l \varepsilon_l\right) \tag{20}$$

where $C_{\varepsilon 1}$=1.44, $C_{\varepsilon 2}$ =1.92, σ_k=1.0, σ_ε =1.3 and P_l, the turbulence production due to viscous and buoyancy forces, is given by

$$P_l = \mu_{tl}\nabla\vec{u}_l.\left(\nabla\vec{u}_l + \nabla\vec{u}_l^{\,T}\right) - \frac{2}{3}\nabla.\vec{u}_l\left(3\mu_{tl}\nabla.\vec{u}_l + \rho_l k_l\right) \tag{21}$$

For the continuous phase (liquid phase) the effective viscosity is calculated as

$$\mu_{eff,l} = \mu_l + \mu_{T,l} + \mu_{tg} + \mu_{ts} \tag{22}$$

where μ_l is the liquid viscosity, $\mu_{T,l}$ is the liquid phase turbulence viscosity or shear induced eddy viscosity, which is calculated based on the k-ε model as

$$\mu_{T,l} = c_\mu \rho_l \frac{k^2}{\varepsilon} \tag{23}$$

μ_{tg} and μ_{ts} represent the gas and solid phase induced turbulence viscosity respectively and are given by

$$\mu_{tg} = c_{\mu p}\rho_l \in_g d_b \left|\vec{u}_g - \vec{u}_l\right| \tag{24}$$

$$\mu_{ts} = c_{\mu p}\rho_l \in_s d_p \left|\vec{u}_s - \vec{u}_l\right| \tag{25}$$

where $C_{\mu p}$ has a value of 0.6.
The effective viscosities of dispersed phases (gas and solid) are calculated as

$$\mu_{eff,g} = \mu_g + \mu_{T,g} \tag{26}$$

$$\mu_{eff,s} = \mu_s + \mu_{T,s} \tag{27}$$

where $\mu_{T,g}$ and $\mu_{T,s}$ are the turbulence viscosity of gas and solid phases respectively. The turbulent viscosity of the gas phase and the solids phase is related to the turbulence viscosity of the continuous liquid phase and are given by equations (28) and (29)

$$\mu_{T,g} = \frac{\rho_g}{\rho_l}\mu_{T,l} \tag{28}$$

$$\mu_{T,s} = \frac{\rho_s}{\rho_l}\mu_{T,l} \tag{29}$$

Closure law for solids pressure

The solids phase pressure gradient results from normal stresses resulting from particle–particle interactions, which become very important when the solid phase fraction approaches the maximum packing. This solid pressure term is defined based on the concept of elasticity, which is described as a function of elasticity modulus and solid volume fraction. The most popular constitutive equation for solids pressure as given by Gidaspow (1994) is

$$\nabla P_s = G(\epsilon_s)\nabla \epsilon_s \tag{30}$$

where G (ε_s) is the elasticity modulus and it is given as

$$G(\epsilon_s) = G_0 \exp\left(c(\epsilon_s - \epsilon_{sm})\right) \tag{31}$$

as proposed by Bouillard et al. (1989), where G_0 is the reference elasticity modulus, c is the compaction modulus and ϵ_{sm} is the maximum packing parameter.

2.2 Impeller rotation modeling

Flows in baffled stirred reactors are modeled by different approaches, which are basically classified into four types (Ranade, 2002). They are black box approach, sliding mesh approach, multiple reference frame or inner–outer approach and computational snapshot approach. The black box approach is basically a steady state approach which requires boundary conditions like mean velocity and turbulence characteristics on the impeller swept surface, and these parameters need to be determined experimentally. This approach cannot be extended easily to multiphase systems since experimental values cannot be obtained accurately and hence this approach cannot be used as a design tool. In the sliding mesh approach, full transient simulations are carried out using two grid zones. One grid zone is attached to the stationary baffles and reactor wall and the other zone is attached to the rotating impeller. The detailed geometry of the impeller needs to be modeled and the impeller blades are modeled as solid rotating walls. The boundary between the two zones should be chosen in such a way that it is greater than the impeller radius but less than the inner edges of the baffles. General transport equations are used for both the zones. This method was first applied to flow in stirred tank by Perng and Murthy (1992). Since this approach is capable of generating a priori predictions, this approach can be used as a design tool. But since this approach requires tremendous computational power, this approach is not widely used as a design tool.

Inner–outer approach or multiple reference frame (MFR) approach, approximates the unsteady flow in stirred vessels. In both the approaches, a fictitious cylindrical zone with radius larger than that of impeller blades and smaller than the inner tip of the baffles and height sufficient to include the entire impeller region is defined. Only difference between inner–outer approach and MFR approach is inner and outer zones overlap in the inner–

outer approach, whereas in the MRF approach there is no overlap. Here also the full geometry needs to be modeled and the impeller blades are modeled as walls. In the MRF approach, flow characteristics of the inner region are solved using a rotating framework. These results are used to provide boundary conditions for the outer region after azimuthal averaging where the flow is solved using a stationary frame work. Solution of outer region is used to provide boundary condition for the inner region. This method was originally introduced by Luo et al. (1994). The inner-outer approach was introduced by Brucato et al. (1994).The fourth approach is called computational snapshot approach which was first proposed by Ranade (1994). This approach is based on taking a snapshot of flow in stirred vessels with a fixed relative position of blades and baffles. In this approach also, the whole solution domain is divided into two regions like in MRF approach, but the time derivative terms in the inner region are approximated in terms of spatial derivatives. The impeller blades are modeled as solid walls and flow is simulated using a stationary framework for a specific blade position. Appropriate sources are specified to consider the impeller rotation. If necessary, simulations are carried out at different blade positions to obtain ensemble-averaged results over different blade positions.

In this work, the MFR approach is used for simulating the impeller rotation. In the MFR approach, the computational domain is divided into an impeller zone (rotating reference frame) and a stationary zone (stationary reference frame). The interaction of inner and outer regions is accounted for by a suitable coupling at the interface between the two regions where the continuity of the absolute velocity is implemented. In this work, the boundary between inner and outer region is located at position of r/R=0.6.

3. Numerical methodology

The commercial CFD software ANSYS CFX-10 is used for the steady state hydrodynamic simulation of multiphase flows in the mechanically agitated contactor. Steady state simulations are performed for different types of impellers, agitation speeds, particle diameter, solid concentration and air flow rate. The details of the reactor geometry used for CFD simulation and the operating parameters are given in Table 3.

Reference	Impeller type	Geometry	Physical Properties	Operating conditions
Guha et al.(2007)	6-DT	T=H=0.2 m D/T=1/3, C/T=1/3	Liquid: ρ = 1000 kg/m^3, Solid: ρ = 2500 kg/m^3, d_p = 300 µm	Solid conc. =7 vol% N_{js}=1200 rpm
Spidla et al.(2005 a, b)	6-PBTD and 4-A315	T=H=1.0 m D/T=1/3, C/T=1/3	Liquid: ρ = 1000kg/m^3, Solid: ρ = 2500kg/m^3, d_p = 350 µm	Solid conc. =10 vol% N_{js} = 267 rpm
Our experiment	6-DT and 4-PBTD	T=H=0.25 m For DT, D = 0.1m, For PBTD, D=0.125 m C/T=0.0625 m	Liquid: ρ = 1000 kg/m^3, Solid: ρ = 4200 kg/m^3, d_p =125, 180, 230 µm Gas: Air	Solid conc. =30 wt% N_{js} = 330–520 rpm Air flow = 0–1.0 vvm

Table 3. Tank design parameters and physical properties

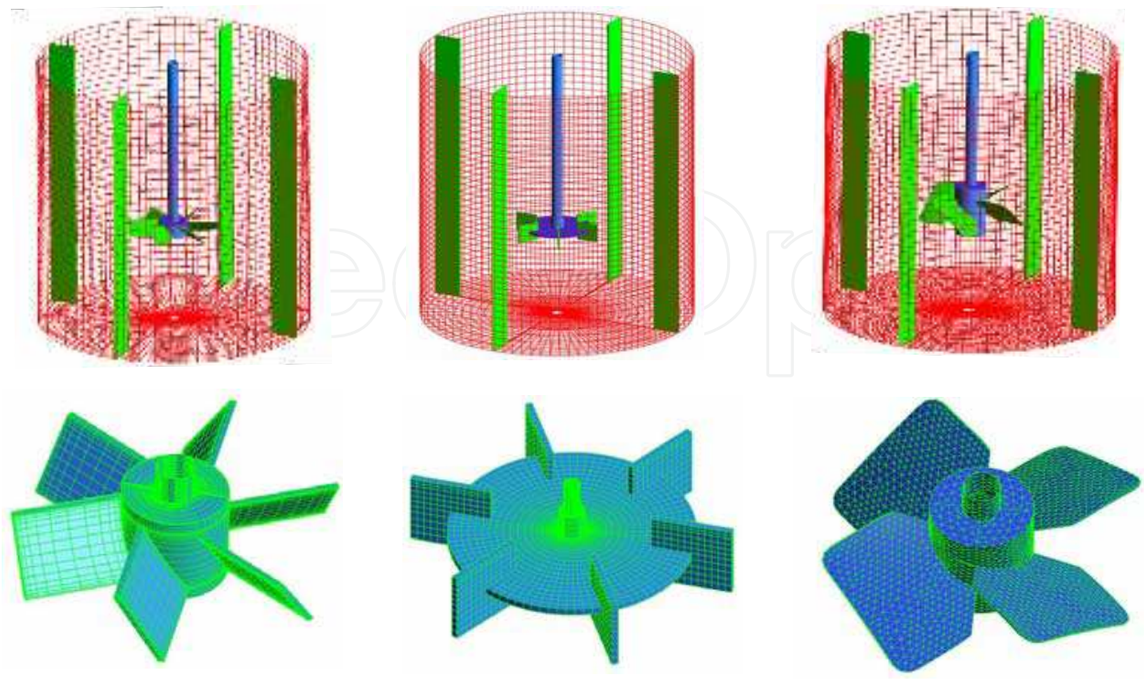

(a) 6 blade Pitched Turbine (b) 6 blade Rushton turbine (c) 4 blade A315 hydrofoil

Fig. 2. Typical geometry and mesh used in the CFD simulation

Due to the symmetry of geometry, only one-half of the agitated contactor is considered as the computational domain and is discretised using block structured grids, which allows finer grids in regions where higher spatial resolutions are required. The blocks are further divided into finer grids. The computational domain is discretised by using ICEM CFD software. Figure 2 depicts a typical mesh used for the numerical simulation. The numerical solutions of set of governing equations described in earlier sections consists of the following steps: (a) translations of partial differential equations into their discretised form in the form of liner algebraic equations (b) using suitable algorithm to handle the various interactions and couplings (c) finally solve the resulting algebraic equations. The discrete algebraic governing equations are obtained by the element based finite volume method. The second order equivalent to high-resolution discretisation scheme is applied for obtaining algebraic equations for momentum, volume fraction of individual phases, turbulent kinetic energy and turbulence dissipation rate. Pressure–velocity coupling was achieved by the Rhie-Chow algorithm (1982). No-slip boundary conditions are applied on the tank walls and shaft. The free surface of tank is considered as the degassing boundary condition. Initially the solid particles are distributed in a homogeneous way inside the whole computational domain. The governing equations are solved using the advanced coupled multi grid solver technology of ANSYS CFX-10. The criteria for convergence is set as 1×10^{-4} for the RMS residual error for all the governing equations. The RMS (Root Mean Square) residual is obtained by taking all of the residuals throughout the domain, squaring them, taking the mean, and then taking the square root of the mean for each equation.

4. Numerical results

4.1. Solid suspension in solid–liquid mechanically agitated reactor

CFD simulation of liquid–solid mechanically agitated contactor is undertaken in this study to verify quantitatively the solid suspension characteristics since this is the vital parameter for predicting the performance of this type of reactor. One way of checking the quality of solid suspension is by evaluating the extent of off-bottom suspension i.e., critical impeller speed for just suspended state. Another way is to map the concentration profiles of solids in such reactors to determine the extent of solid distribution i.e., solid suspension height.

4.1.1 Off-bottom suspension

Generally Zwietering criteria (the impeller speed at which the particles do not remain stationary at the bottom of the vessel for more than 2 s) is used for characterising the off-bottom suspension. But incorporating Zwietering criteria is difficult in the Eulerian–Eulerian approach of the present CFD simulation. Hence the method proposed by Bohnet and Niesmak (1980), which is based on the value of standard deviation, is used in the present study for the prediction of critical impeller speed. This standard deviation method was also successfully employed for liquid–solid suspension by Khopkar et al. (2006). It is defined as

$$\sigma = \sqrt{\frac{1}{n}\sum_{i=1}^{n}\left(\frac{C_i}{C_{avg}} - 1\right)^2} \tag{32}$$

where n is the number of sampling locations which is used for measuring the solid holdup. The increase in the degree of homogenisation (better suspension quality) is manifested in the reduction in the value of the standard deviation. The standard deviation is broadly divided into three ranges based on the quality of suspension. For uniform suspension the value of the standard deviation σ is found to be smaller than 0.2 ($\sigma<0.2$), for just suspended condition the value of the standard deviation is between 0.2 and 0.8 ($0.2<\sigma< 0.8$) and for an incomplete suspension the standard deviation value is greater than 0.8 ($\sigma > 0.8$). But it is very difficult to exactly find the critical impeller speed required for the just suspended state from the values of the standard deviation. These difficulties were also cited in literature (Khopkar et al., 2006, van der Westhuizen & Deglon 8). Hence we have also used another criterion which is based on the solid suspension height i.e., cloud height ($H_{cloud}= 0.9H$) along with the standard deviation method. Kraume (1992) used these two criteria to determine the critical impeller speed in liquid–solid suspension. For the present study, both these criteria have been used to evaluate the quality of solid suspension and to determine the critical impeller speed.

CFD simulations have been carried out for the reactor configuration of Spidla et al. (2005a) for three different impeller types. Figure 3 shows the variation of the standard deviation values with respect to the impeller speed for DT, PBTD and A315 hydrofoil impeller. The standard deviation value decreases with an increase in impeller speed for all the impellers. Figure 4 depicts the predicted cloud height for various impeller rotational speeds (4.0, 4.45, and 5.0 rps) for the PBTD impeller. Figure 5 depicts the predicted cloud height for various impeller rotational speeds (3.5, 4.1, and 4.7 rps) for the A315 hydrofoil impeller. It can be

seen clearly from these figures that there is an increase in the cloud height with an increase in the impeller speed. Similar observations were also reported by Khopkar et al. (2006).

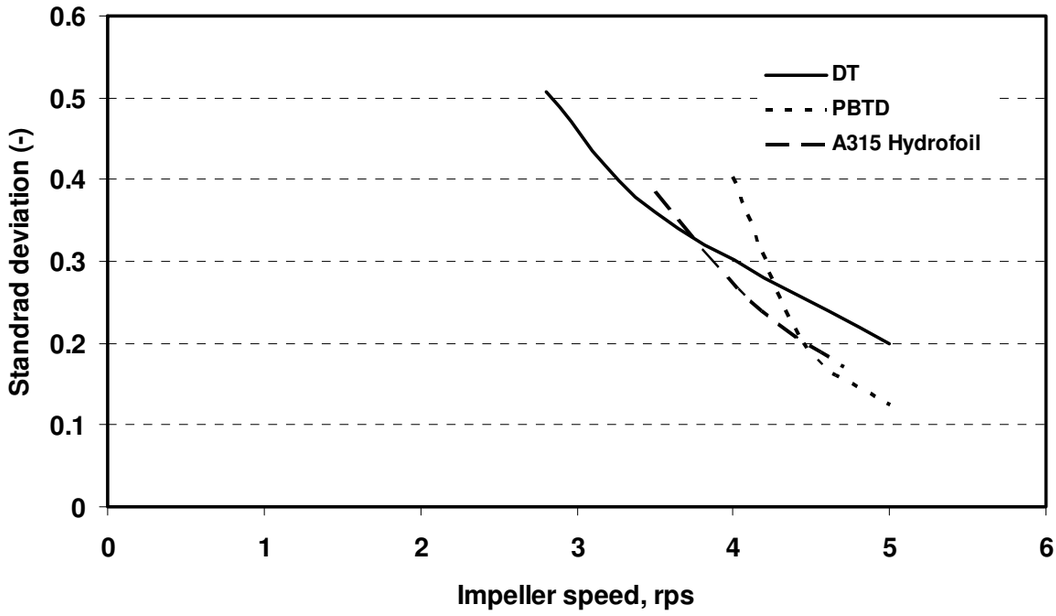

Fig. 3. Standard deviation values obtained from CFD with respect to impeller rotational speed for DT, PBTD and A315 hydrofoil impeller (particle size of 350 μm with solids loading of 10 vol. %)

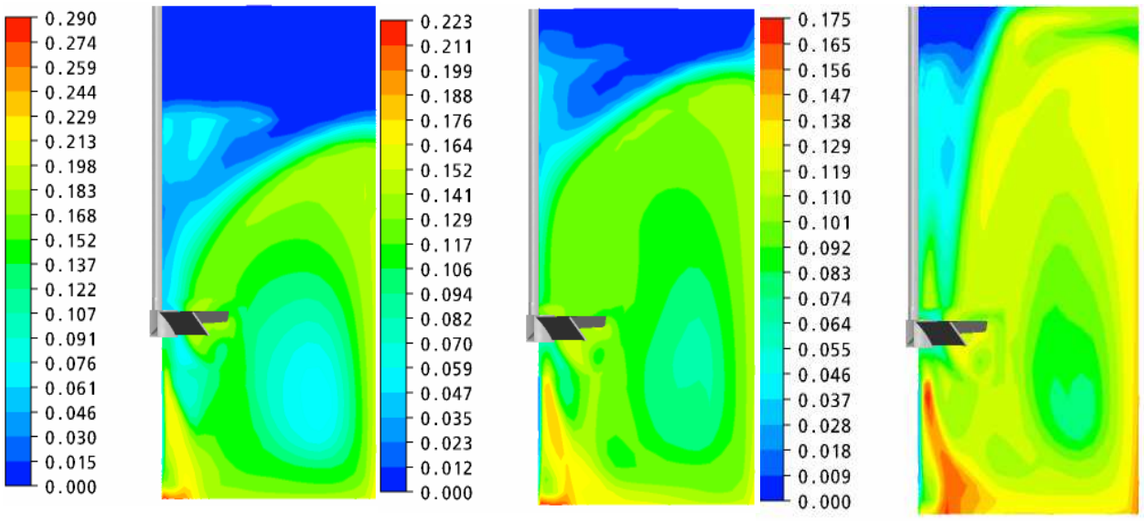

(a) 4 rps (H_s/H=0.8) (b) 4.45 rps (H_s/H=0.9) (c) 5 rps (H_s/H=1.0)

Fig. 4. Cloud height predicted by CFD simulation for PBTD impeller at different rotational speeds (particle size of 350 μm with solid loading of 10 vol. %)

The values of the standard deviation and cloud height obtained by CFD simulation along with experimental values for the three types of impellers are presented in Table 4. Based on

these two criteria, it is found that the critical impeller speed required for 6-PBTD is 4.45 rps which agrees very well with the experimental observation. It has to be noted again that both these criteria have to be satisfied for the determination of the critical impeller speed.

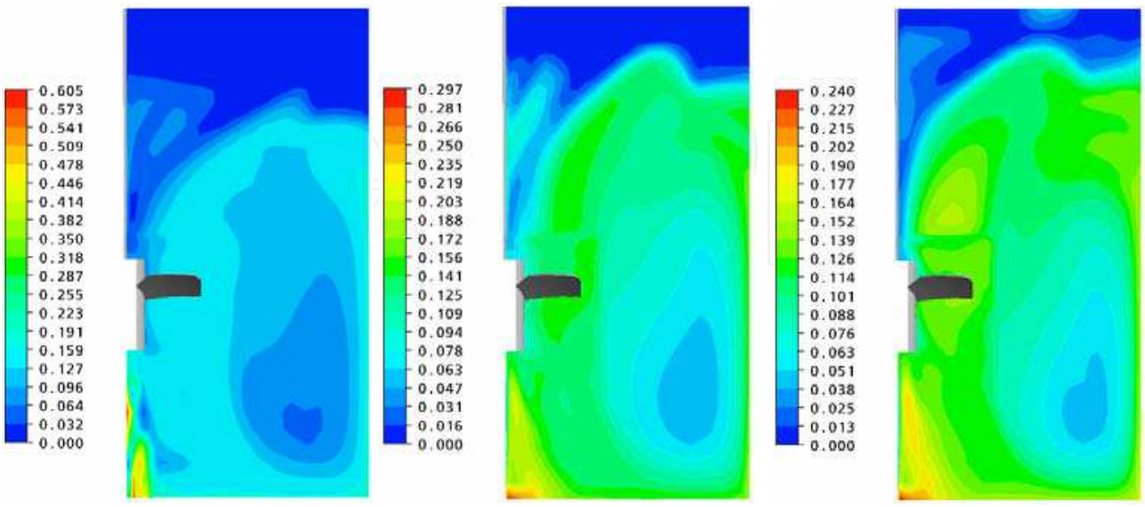

(a) 3.5 rps (H_s/H=0.8) (b) 4.1 rps (H_s/H=0.88) (c) 4.7rps (H_s/H=1.0)

Fig. 5. Cloud height predicted by CFD simulation for A315 hydrofoil impeller at different rotational speeds (particle size of 350 μm with solid loading of 10 vol. %)

Type of impeller	Critical impeller speed, rps		Standard deviation, σ	Cloud height
	Experimental (rps)	CFD (rps)		
DT	-	3.5	0.36	0.90
PBTD	4.45	4.45	0.21	0.91
A315 hydrofoil	-	4.1	0.25	0.88

Table 4. Effect of impeller type on the quality of suspension (particle size of 350 μm with solid loading of 10 vol. %)

4.1.2 Power number comparison

The comparison of different types of impellers with regard to their suspension ability is investigated in terms of power number. The power consumption is calculated as the product of torque on the impeller blades and the angular velocity. This is then used for the estimation of power number which is expressed as follows:

$$N_P=2\pi NT/\rho_s N^3 D^5 \quad (33)$$

where torque (T) exerted on all blades was computed from the total momentum vector, which is computed by summing the cross products of the pressure and viscous forces vectors for each facet on the impeller with the moment vector.

The predicted values of power number are compared with experimental data and are shown in Table 5. It can be observed that the values predicted by CFD simulations agree reasonably

well with the experimental values. It can also be seen from the table that the suspension performance in terms of power number is different for different impeller designs. The lowest power consumption was observed for A315 hydrofoil impeller and highest for Rushton turbine impeller. This indicates that the impeller which directs the flow downward having mainly axial component and has the least power number is most energy efficient.

Impeller type	Power number	
	Experimental	CFD
6-Rushton turbine	6.0	5.1
6-PBTD	1.67	1.55
4- A315 Hydrofoil downward	1.5	1.37

Table 5. Experimental and predicted values of Power number

4.2 Solid suspension in gas–solid–liquid mechanically agitated reactor

The critical impeller speed for gas–liquid–solid mechanically agitated contactor obtained by CFD simulation based on the criteria of both standard deviation approach and cloud height is validated with our experimental data. The bubble size distribution in the mechanically agitated reactor depends on the design and operating parameters and there is no experimental data available for bubble size distribution. It has been reported by Barigou and Greaves (1992) that their bubble size distribution is in the range of 3.5–4.5 mm for the higher gas flow rates used in their experiments. Also in the recent simulation study on a gas–liquid stirred tank reactor carried out by Khopkar et al. (2005) a single bubble size of 4 mm was assumed. Since the gas flow rates used in our experiments are also in the same range, a mean bubble size of 4 mm is assumed for all our simulations.

4.2.1 Off-bottom suspension

CFD simulations have been carried out for 6 blade Rushton turbine impeller (DT) and 4 blade pitched blade turbine with downward pumping (PBTD) at different impeller speeds. The air flow rate for this simulation is 0.5 vvm and the solid phase consists of ilmenite particles of size 230 μm and the solid loading is 30% by weight. Figure 6 shows the variation of the standard deviation value with respect to impeller speed for DT and PBTD. The value of standard deviation decreases with increase in impeller speed for both the impellers. Figure 7 depicts the predicted cloud height for the three impeller rotational speeds (7.83, 8.67, and 9.5 rps) for DT and Figure 8 shows the predicted cloud height for PBTD for three different impeller speeds (6.3, 7.13, and 7.97 rps). It can be seen clearly from these figures that there is an increase in the cloud height with an increase in the impeller rotational speed. Similar observations were also reported by Khopkar et al. (2006). The values of standard deviation and cloud height obtained by CFD simulation along with experimental values for both the type of impellers are presented in Table 6. Based on these two criteria, it is found that the critical impeller speed required for DT is 8.67 rps and for PBTD is 7.13 rps which agrees very well with the experimental observation. It has to be noted again that both the criteria have to be satisfied for critical impeller speed determination.

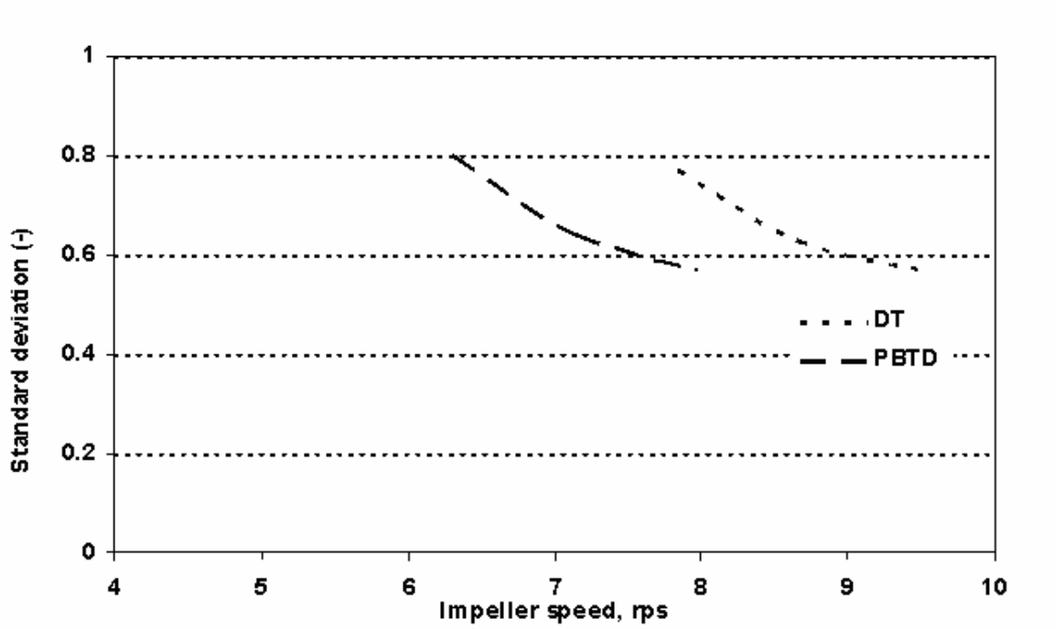

Fig. 6. Variation of standard deviation values with respect to the impeller speed for DT and PBTD

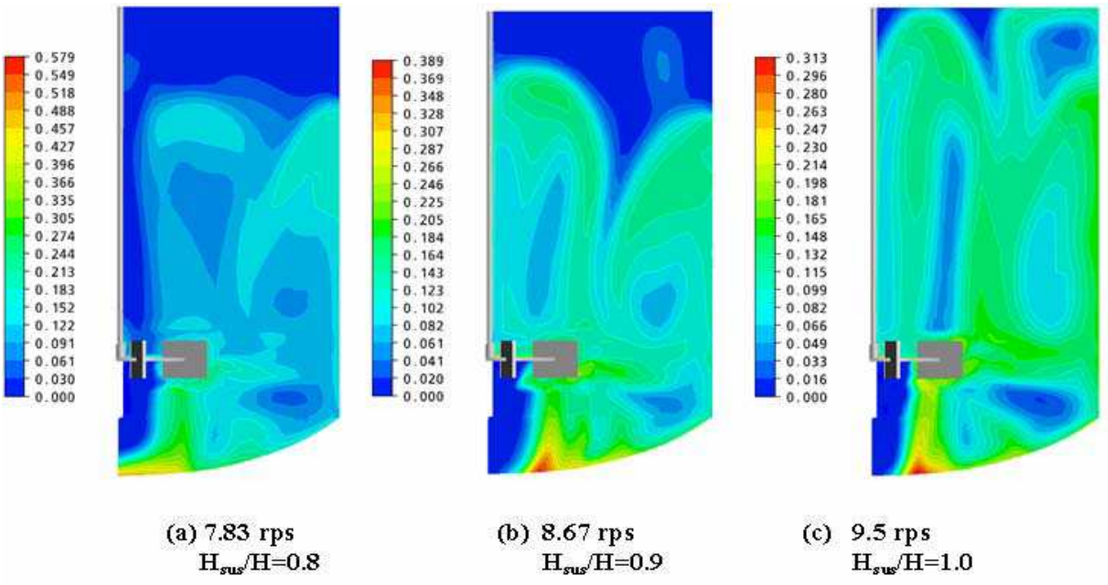

Fig. 7. CFD prediction of cloud height with respect to the impeller speed for DT (gas flow rate = 0.5 vvm, particle size = 230 μm & particle loading = 30 wt.%)

4.2.1 Effect of particle size

It has been reported in the literature that the critical impeller speed depends on the particle size. Hence, CFD simulations have been carried out for three different particle sizes *viz,* 125 μm, 180 μm and 230 μm at the solid loading of 30 % by wt. and a gas flow rate of 0.5 vvm with both DT and PBTD type impellers. From the CFD simulation, the standard deviation

and cloud height values are also obtained and they are shown in Table 7. It can be seen clearly that critical impeller speed predicted by CFD simulation based on the criteria of standard deviation and solid cloud height agrees very well with the experimental data.

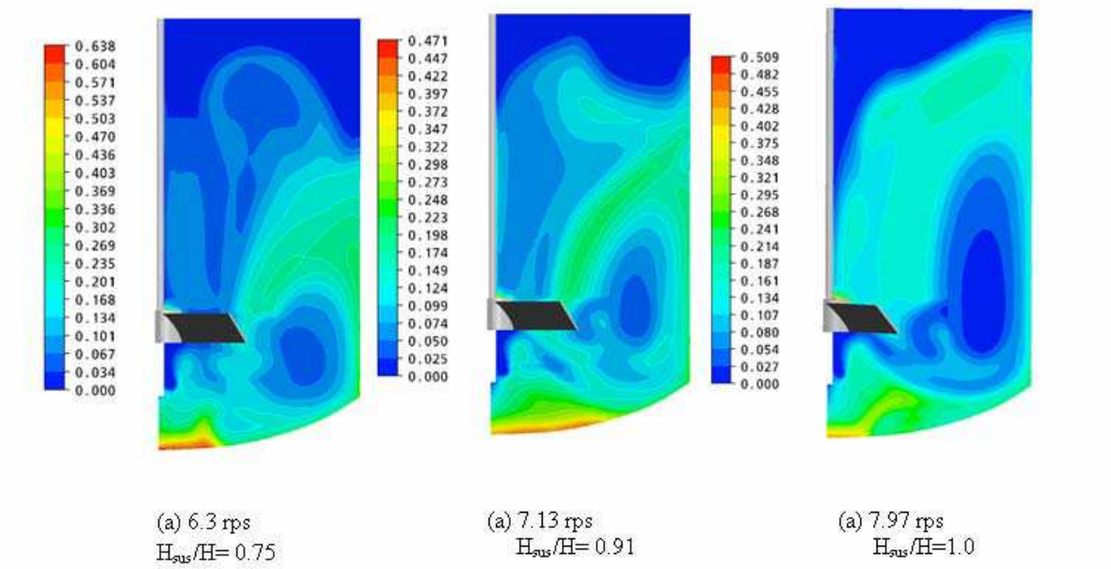

Fig. 8. CFD prediction of cloud height with respect to the impeller speed for PBTD (gas flow rate = 0.5 vvm, particle size =230 μm & particle loading =30 wt %)

Type of impeller	Critical impeller speed, rps		Standard deviation, σ	Cloud height
	Experimental	CFD simulation		
DT	8.67	8.67	0.66	0.90
PBTD	7.13	7.13	0.64	0.91

Table 6. Effect of impeller type on quality of suspension (gas flow rate =0.5 vvm, particle size = 230 μm, & particle loading = 30 wt %)

Particle diameter (μm)	(DT)				PBTD			
	Critical impeller speed, rps		Standard deviation, σ	Cloud height	Critical impeller speed, rps		Standard deviation, σ	Cloud height
	Experimental	CFD			Experimental	CFD		
125	5.67	5.67	0.50	0.90	5.42	5.42	0.46	0.91
180	6.25	6.92	0.75	0.89	5.77	6.0	0.62	0.88
230	8.67	8.67	0.66	0.90	7.13	7.13	0.64	0.91

Table 7. Effect of particle size on quality of suspension (gas flow rate = 0.5 vvm & particle loading 30 = wt %)

4.2.2 Effect of air flow rate

CFD simulations have further been carried out to study the effect of air flow rate on the critical impeller speed for gas–liquid–solid mechanically agitated contactor. Figure 9 shows the comparison of CFD predictions with the experimental data on critical impeller speed for both the type of impellers at various gas flow rates (0 vvm, 0.5 vvm and 1. 0 vvm). The values of the standard deviation and cloud height with respect to the impeller speed for different gas flow rates with different type of impellers are shown in Table 8. It can be observed that CFD simulation is capable of predicting the critical impeller speed in terms of standard deviation value and cloud height with an increase in gas flow rate for both types of impellers. Figure 10 shows solid volume fraction distribution predicted by CFD at the critical impeller speed for the solid loading of 30 % by wt. and particle size of 230 μm with different air flow rates (0, 0.5, 1.0 vvm).

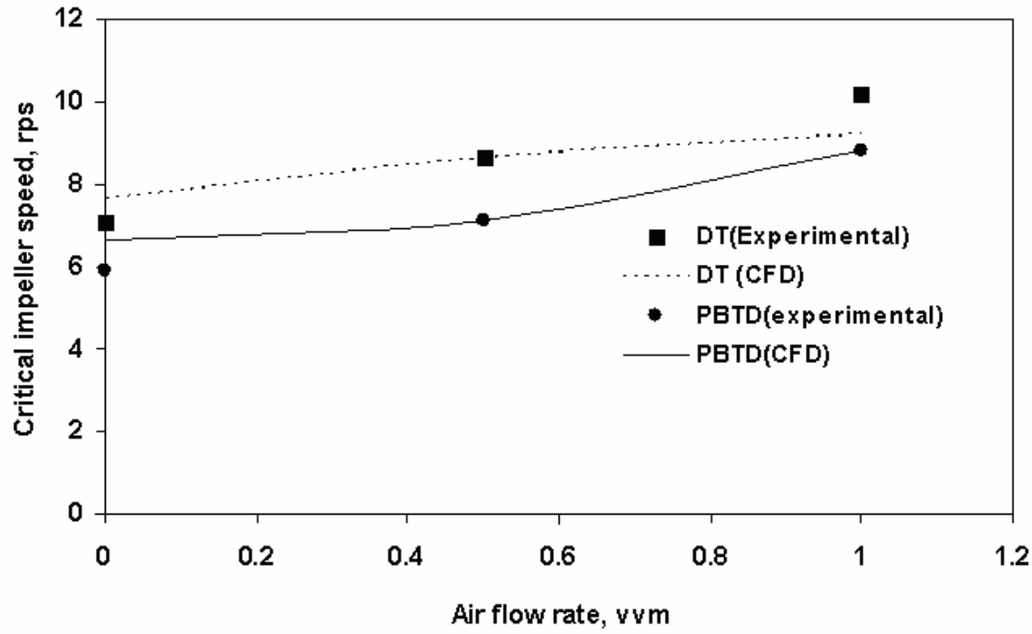

Fig. 9. Effect of air flow rate on Critical impeller speed for different impellers (particle size= 230 μm & particle loading = 30 wt %)

Air flow rate (vvm)	DT				PBTD			
	Critical impeller speed, rps		Standard deviation, σ	Cloud height	Critical impeller speed, rps		Standard deviation, σ	Cloud height
	Experimental	CFD			Experimental	CFD		
0	7.17	7.67	0.80	0.89	5.5	6.67	0.80	0.90
0.5	8.67	8.67	0.66	0.90	7.13	7.13	0.64	0.91
1.0	10.2	9.2	0.66	0.90	8.82	8.82	0.71	0.93

Table 8. Effect of air flow rate on quality of suspension for different type of impellers (particle size = 230 μm & particle loading = 30 wt. %)

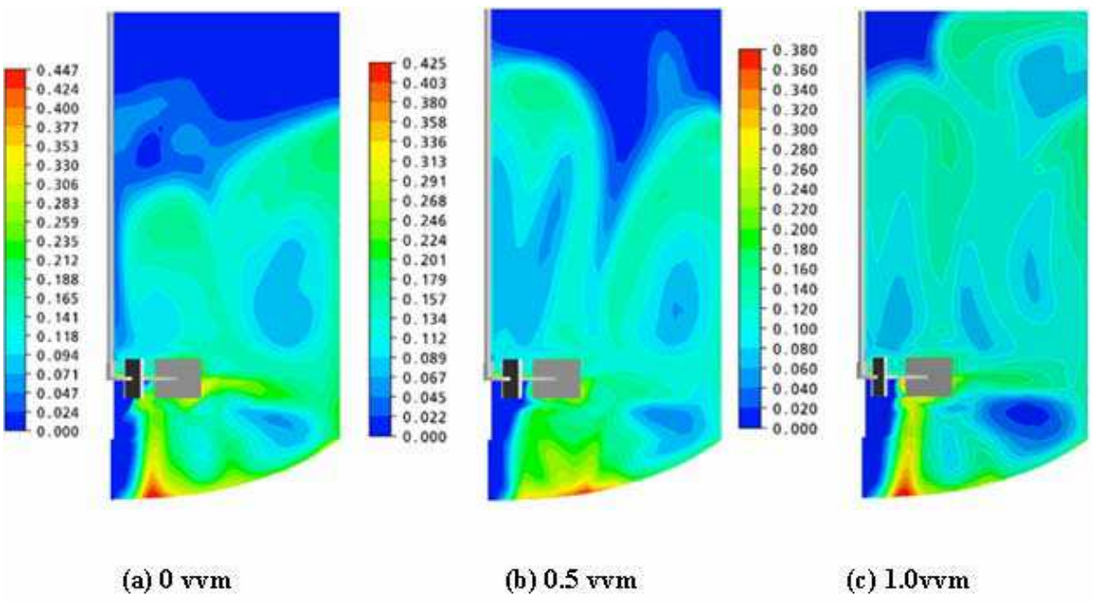

Fig. 10. Effect of air flow rate on solid concentration distribution for DT by CFD simulations at the critical impeller speed (a) 0 vvm (b) 0.5 vvm (c) 1. 0 vvm (particle size =230 μm and particle loading = 30 wt. %)

Figure 11 shows the variation of standard deviation value with respect to the impeller speed. It can be seen that the reduction rate of standard deviation value in ungassed condition is more with increasing impeller speed when compared with gassed condition. Similarly for the case of higher gas flow rate, the reduction rate in the standard deviation value is much lower compared to lower gas flow rate. This is due to the presence of gas which reduces both turbulent dispersion and fluid circulation action of the impeller.

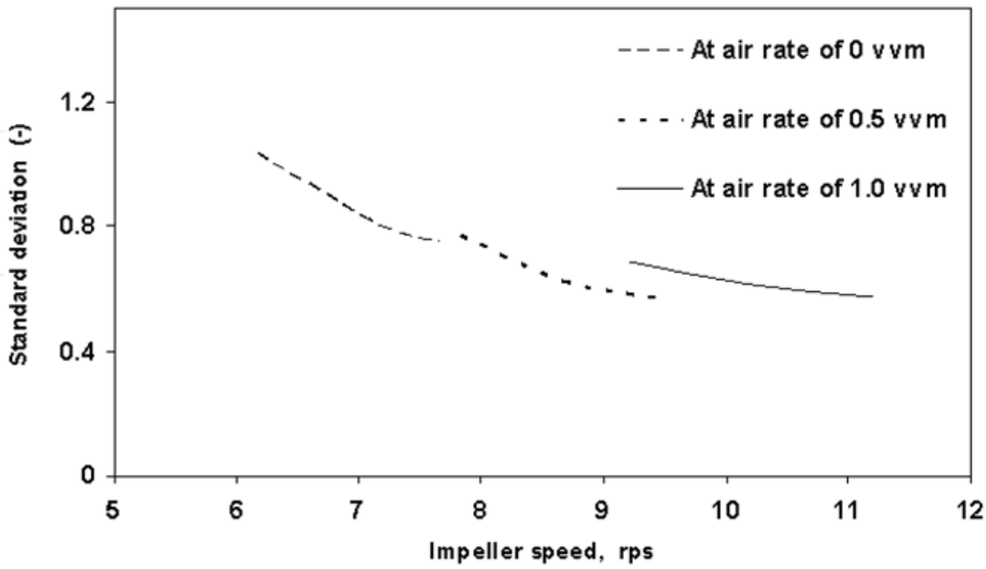

Fig. 11. Effect of gas flow rate on the standard deviation value for different impeller speeds of DT (particle size= 230 μm &particle loading= 30 wt.%)

5. Conclusions

In this present work, Eulerian multi-fluid approach along with standard k-ε turbulence model has been used to study the solid suspension in liquid-solid and gas–liquid–solid mechanically agitated contactor. CFD predictions are compared quantitatively with literature experimental data (Spidla et al., 2005a,b) in terms of critical impeller speed based on the criteria of standard deviation method and cloud height in a mechanically agitated contactor. An adequate agreement was found between CFD prediction and the experimental data. The numerical simulation has further been extended to study the effect of impeller design (DT, PBTD and A315 Hydrofoil), impeller speed and particle size (200–650 μm) on the solid suspension in liquid–solid mechanically agitated contactor.

For gas–liquid–solid flows, the CFD predictions are compared quantitatively with our experimental data in terms of critical impeller speed based on the criteria of standard deviation method and cloud height in a mechanically agitated contactor. An adequate agreement was found between CFD prediction and experimental data. The numerical simulation has further been extended to study the effect of impeller design (DT, PBTD), impeller speed, particle size (125–230 μm) and air flow rate (0–1.0 vvm) on the prediction of critical impeller speed for solid suspension in gas–liquid–solid mechanically agitated contactor.

Nomenclature

c	solid compaction modulus
C_{avg}	average solid concentration
C_i	instantaneous solid concentration
$C_{D,ls}$	drag coefficient between liquid and solid phase
$C_{D,lg}$	drag coefficient between liquid and gas phase
C_D	drag coefficient in turbulent liquid
C_{D0}	drag coefficient in stagnant liquid
C_{TD}	turbulent dispersion coefficient
$C_\mu, \sigma_k, \sigma_\varepsilon, C_{\varepsilon 1}, C_{\varepsilon 2}$	coefficient in turbulent parameters
$C_{\mu p}$	coefficient in particle induced turbulence model
D	impeller diameter, m
d_b	bubble mean diameter, m
d_p	particle mean diameter, m
Eo	Eotvos number
F_{TD}	turbulent Dispersion Force, N
$F_{D,lg}$	interphase drag force between liquid and gas, N
$F_{D,ls}$	interphase drag force between liquid and solid, N
g	acceleration due to gravity, m / s^2
$G(\in_s)$	solid elastic modulus
G_0	reference elasticity modulus
H_{cloud}	Cloud height, m
k	the turbulence kinetic energy, m^2/s^2
n	number of sampling locations
N	impeller speed, rpm
N_{js}	critical impeller speed for just suspended, rpm

N_{jsg}	critical impeller speed in the presence of gas, rpm
N_P	Power number
N_q	Pumping number
P	Power, W
P	liquid-phase pressure, kg/ m^1 s^2
P_s	solids pressure, kg /m s^2
P_α	turbulence production due to viscous and buoyancy forces
Q_g	gas flow rate, vvm
R	radial position, m
Re_b	bubble Reynolds number
Re_p	particle Reynolds number
T	Tank height, m
$\vec{u}_g$	local gas phase velocity vector, m/s
$\vec{u}_l$	local liquid phase velocity vector, m/s
$\vec{u}_s$	local solid phase velocity vector, m/s
z	axial position, m

Greek letters

$\epsilon_l, \epsilon_g, \epsilon_s$	liquid, gas and solid volume fraction respectively
ϵ_{sm}	maximum solid packing parameter
ε, ε_l	liquid phase turbulence eddy dissipation, m^2/s^3
ρ_g	gas density, kg/m^3
ρ_l	liquid density, kg/m^3
ρ_s	density of solid phase, kg/ m^3
$\Delta\rho$	density difference between liquid and gas, kg/m^3
ΔN_{js}	Difference in critical impeller speed, rpm
$\mu_{eff,c}$	continues phase effective viscosity, kg /m s^2
$\mu_{eff,d}$	dispersed phase effective viscosity, kg /m s^2
μ_c	continuous viscosity, kg /m s^2
μ_d	dispersed phase viscosity, kg /m s^2
μ_{td}	dispersed phase induced turbulence viscosity, kg /m s^2
$\mu_{\tau,c}$	continuous phase turbulent viscosity, kg /m s^2
σ	standard deviation value for solid suspension

Subscripts and superscripts

k	phase
s	solid phase
l	liquid phase
g	gas phase
eff	effective
max	maximum
DT	Disc turbine
PBTD	Pitched blade turbine downward pumping
PBTU	Pitched blade turbine upward pumping
rpm	revolution per minute
vvm	volume of gas per volume of liquid per minute

6. References

Armenante, P.M., Nagamine, E.U., 1998. Effect of low off-bottom impeller clearance on the minimum agitation speed for complete suspension of solids in stirred tanks. Chemical Engineering Science 53, 1757–1775.

Baldi, G., Conti, R., Alaria, E., 1978. Complete suspension of particles in mechanically agitated vessels. Chemical Engineering Science 33, 21–25.

Bakker, A., Fasano, J.B., Myers, K.J., 1994. Effects of flow pattern on the solids distribution in a stirred tank. Institution of Chemical Engineering Symposium Series 136, 1–8.

Barrue, H., Bertrand, J., Cristol, B., Xuereb, C., 2001. Eulerian simulation of dense solid–liquid suspension in multi-stage stirred vessel. Journal of Chemical Engineering Japan. 34, 585–594.

Barigou, M., Greaves, M., 1992. Bubble size distribution in a mechanically agitated gas–liquid contactor. Chemical Engineering Science 47, 2009–2025.

Bohnet, M., Niesmak, G., 1980. Distribution of solids in stirred suspension. General Chemical Engineering 3, 57-65.

Bouillard, J.X., Lyczkowski, R.W., Gidaspow, D., 1989. Porosity distribution in a fluidised bed with an immersed obstacle. A.I.Ch.E. Journal 35, 908–922.

Brucato, A., Ciofalo, M., Grisafi, F., Micale, G., 1994. Complete numerical simulation of flow fields in baffled stirred vessels: the inner-outer approach. Institution of Chemical Engineering Symposium Series 136, 155–162.

Brucato, A., Grisafi, F., Montante, G., 1998. Particle drag coefficient in turbulent fluids. Chemical Engineering Science 53, 3295–3314.

Bujalski, W., Konno. M., Nienow, A.W., 1988. Scale-up of 45° pitch-blade agitators for gas dispersion and solid suspension. Proceeding of 6th European Conference on Mixing, Italy, 389–398.

Bujalski, W., Takenaka, K., Paolini, S., Jahoda, M., Paglianti, A., Takahashi, K., Nienow, A.W., Etchells, A.W., 1999. Suspension and liquid homogenization in high solids concentration stirred chemical reactors. Chemical Engineering Research and Design 77, 241–247.

Chapman, C.M., Nienow, A.W., Cooke, M., Middleton, J.C., 1983a. Particle–gas–liquid mixing in stirred vessels, part I: particle–liquid mixing. Chemical Engineering Research and Design 61a, 71–81.

Chapman, C.M., Nienow, A.W., Cooke, M.; Middleton, J.C. 1983b. Particle–gas–liquid mixing in stirred vessels, part III: three-phase mixing. Chemical Engineering Research and Design 61a, 167–181.

Chudacek, M.W., 1986. Relationships between solids suspension criteria, mechanism of suspension, tank geometry, and scale-up parameters in stirred tanks. Industrial and Engineering Chemistry Fundamentals 25, 391–401.

Dohi, N., Takahashi, T., Minekawa, K., Kawase, Y., 2004. Power consumption and solid suspension performance of large-scale impellers in gas–liquid–solid three-phase stirred tank reactors. Chemical Engineering Journal 97, 103–114.

Dutta, N.N., Pangarkar, V.G., 1995. Critical impeller speed for solid suspension in multi-impeller three-phase agitated contactors. The Canadian Journal of Chemical Engineering 73, 273–283.

Dudukovic, M.P., Larachi, F., Mills, P.L., 1999. Multiphase Reactor–Revisited. Chemical Engineering Science 54, 1975–1995.

Dylag, M., Talaga, J., 1994. Hydrodynamics of mechanical mixing in a three-phase liquid-gas-solid System. International Chemical Engineering 34, 539–551.

Einenkel, W.G., 1979. Description of fluid dynamics in stirred tanks. VDI Forschungsheft No. 595.

Frijlink, J.J., Bakker, A., Smith, J.M., 1990. Suspension of solid particles with gassed impellers. Chemical Engineering Science 45, 1703–1718.

Gidaspow, D., 1994. Multiphase Flow and Fluidisation: Continuum and Kinetic Theory Descriptions. Academic Press, San Diego.

Guha, D., Ramachandran, P.A., Dudukovic, M.P., 2007. Flow field of suspended solids in a stirred tank reactor by Lagrangian tracking. Chemical Engineering Science 62, 6143–6154

Guha, D., Ramachandran, P.A., Dudukovic, M.P., Derksen, J.J., 2008. Evaluation of large eddy simulation and Euler–Euler CFD Models for solids flow dynamics in a stirred tank reactor. A.I.Ch.E. Journal, 54, 766–778.

Ibrahim, S., Nienow, A. W., 1996. Particle suspension in the turbulent regime: the effect of impeller type and impeller/vessel configuration. Chemical Engineering Research and Design 74a, 679–688.

Kee, N.C.S., Tan, R.B. H., 2002. CFD simulation of solids suspension in mixing vessels. The Canadian Journal of Chemical Engineering 80, 1–6.

Khopkar, A.R., Aubin, J., Xureb, C., Le Sauze, N., Bertrand, J. and Ranade, V.V., 2003. Gas–liquid flow generated by a pitched blade turbine: PIV measurements and CFD simulations. Industrial and Engineering Chemistry Research, 42, 5318–5332.

Khopkar, A.R., Rammohan, A.R., Ranade, V.V., Dudukovic, M.P., 2005. Gas–liquid flow generated by a Rushton turbine in stirred vessel: CARPT/CT measurements and CFD simulations. Chemical Engineering Science 60, 2215–2229.

Khopkar, A.R., Kasat, G.R., Pandit, A.B. and Ranade, V.V., 2006, Computational fluid dynamics simulation of the solid suspension in a stirred slurry reactor. Industrial and Engineering Chemistry Research 45, 4416–4428.

Kolar, V., 1967. Contribution to the theory of suspension and dissolution of granular solids in liquids by means of mechanically mixed liquids. Collection of Czechoslovak Chemical Communications 32, 526–534.

Kraume, M., 1992. Mixing times in stirred suspension. Chemical Engineering and Technology 15, 313–318.

Ljungqvist, M., Rasmuson, A., 2001. Numerical simulation of the two-phase flow in an axially stirred vessel. Chemical Engineering Research and Design 79, 533–546.

Lopez de Bertodano, M., 1992. Turbulent Bubbly Two-Phase Flow in a Triangular Duct. Ph.D. Thesis, Rensselaer Polytechnic Institute, Troy, New York.

Luo, J. Y., Issa, R. I. and Gosman, A. D., 1994. Prediction of impeller-induced flows in mixing vessels using multiple frames of reference. Institution of Chemical Engineers Symposium Series 136, 549–556.

Micale, G., Montante, G., Grisafi, F., Brucato, A., Godfrey, J., 2000. CFD simulation of particle distribution in stirred vessels. Chemical Engineering Research and Design 78, 435–444.

Montante, G., Magelli, F., 2005. Modeling of solids distribution in stirred tanks: Analysis of simulation strategies and comparison with experimental data. International Journal of Computational Fluid Dynamics 19, 253–262.

Murthy, B.N., Ghadge, R.S., Joshi, J.B., 2007. CFD simulations of gas–liquid–solid stirred reactor: Prediction of critical impeller speed for solid suspension. Chemical Engineering Science 62, 7184–7195.

Narayanan, S., Bhatia, V.K., Guha, D.K., Rao, M.N., 1969. Suspension of solid by mechanical agitation. Chemical Engineering Science 24, 223–230.

Nienow, A.W., 1968. Suspension of solid particles in turbine agitated baffled vessel. Chemical Engineering Science 23, 1453–1459.

Nienow, A.W., Konno. M., Bujalski, W., 1985. Studies on three-phase mixing: A review and recent results. Proceeding of 5th European Conference on Mixing, Wurzburg, Germany, 1–12.

Pantula, P.R.K., Ahmed, N., 1998. Solid suspension and gas hold-up in three phase mechanically agitated reactors. Proceedings of the 26th Australian Chemical Engineering Conference (Chemiea 98), Port Douglas, Australia.

Perng, C.Y., Murthy, J.Y., 1993. A moving-deforming mesh technique for the simulation of flow in mixing tanks. A.I.Ch.E. Symposium Series. 89 (293), 37–41.

Ranade, V.V., Van den Akker, H.E.A., 1994. A computational snapshot of gas-liquid flow in baffled stirred reactors. Chemical Engineering Science 49, 5175–5192.

Ranade, V. V. Computational Flow Modelling for Chemical Reactor Engineering; Academic Press: New York, 2002.

Raghava Rao, K.S.M.S., Rewatkar, V.B., Joshi, J.B., 1988. Critical impeller speed for solid suspension in mechanically agitated contactors. A.I.Ch.E Journal 34, 1332–1340.

Raw, M. J., 1994. A Coupled Algebraic Multigrid Method for the 3-D Navier Stokes Equations. Proceedings of the 10th GAMM-Seminar, Notes on Numerical Fluid Mechanics 49, 204.

Rieger, F., Ditl. P., 1994. Suspension of solid particles. Chemical Engineering Science 49, 2219–2227.

Rewatkar, V.B., Raghava Rao, K.S.M.S., Joshi, J.B., 1991. Critical impeller speed for solid suspension in mechanically agitated three-phase reactors. 1. Experimental part. Industrial and Engineering Chemistry Research 30, 1770–1784.

Rhie, C.M., Chow, W.L., 1982. A numerical study of the turbulent flow past an isolated airfoil with trailing edge separation. AIAA Journal 21, 1525–1532.

Sharma, R.N., Shaikh, A.A., 2003. Solids suspension in stirred tanks with pitched blade turbines. Chemical Engineering Science 58, 2123–2140.

Sha, Z., Palosaari, S., Oinas, P., Ogawa, K., 2001. CFD simulation of solid suspension in a stirred tank. Journal of Chemical Engineering of Japan 34, 621–626.

Shamlou, P.A., Koutsakos, E., 1989. Solids suspension, distribution in liquids under turbulent agitation, Chemical Engineering Science 44, 529–542.

Smith, J. M., 1990. Industrial Needs for Mixing Research. Transactions of Institution of Chemical Engineering 68, 3–6.

Spidla, M., Sinevic, V., Jahoda, M., Machon, V., 2005a. Solid particle distribution of moderately concentrated suspensions in a pilot plant stirred vessel. Chemical Engineering Journal 113, 73–82.

Spidla, M., Sinevic, V., Machon, V., 2005b. Effect of baffle design on the off-bottom suspension characteristics of axial-flow impellers in a pilot-scale mixing vessel. Chemical and Biochemical Engineering Quarterly 19, 333–340.

Takahashi, K., Fujita, H., Yokota, T., 1993. Effect of size of spherical particle on complete suspension speed in agitated vessels of different scale. Journal of Chemical Engineering of Japan 26, 98–100.

van der Westhuizen, A.P., Deglon, D.A., 2008. Solids suspension in a pilot-scale mechanical flotation cell: A critical impeller speed correlation. Mineral Engineering 21, 621–629.

Warmoeskerken, M.M.C.G., van Houwelingen, M.C., Frijlink, J.J., Smith, J.M., 1984. Role of cavity formation in stirred gas–liquid–solid reactors. Chemical Engineering Research and Design 62, 197–200.

Wong, C.W., Wang, J.P. Haung, S.T., 1987. Investigations of fluid dynamics in mechanically stirred aerated slurry reactors. The Canadian Journal of Chemical Engineering 65, 412–419.

Zlokarnik, N.W., Judat, P., 1969. Tubular and propeller stirrers–an effective stirrer combination for simultaneous gassing and suspending. Chemie Ingenieur Technik 41, 1270–1277.

Zhu, Y., Wu, J., 2002. Critical impeller speed for suspending solids in aerated agitation tanks. The Canadian Journal of Chemical Engineering 80, 1–6.

Zwietering, T.N., 1958. Suspending of solid particles in liquid by agitators. Chemical Engineering Science 8, 244–253.

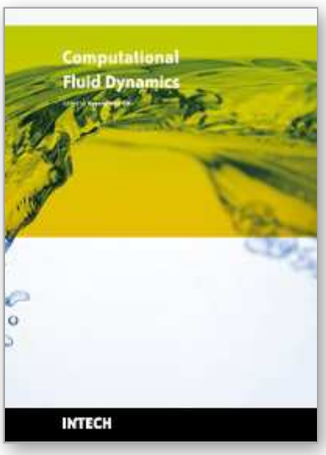

Computational Fluid Dynamics

Edited by Hyoung Woo Oh

ISBN 978-953-7619-59-6
Hard cover, 420 pages
Publisher InTech
Published online 01, January, 2010
Published in print edition January, 2010

This book is intended to serve as a reference text for advanced scientists and research engineers to solve a variety of fluid flow problems using computational fluid dynamics (CFD). Each chapter arises from a collection of research papers and discussions contributed by the practiced experts in the field of fluid mechanics. This material has encompassed a wide range of CFD applications concerning computational scheme, turbulence modeling and its simulation, multiphase flow modeling, unsteady-flow computation, and industrial applications of CFD.

How to reference

In order to correctly reference this scholarly work, feel free to copy and paste the following:

Panneerselvam Ranganathan and Sivaraman Savithri (2010). Computational Flow Modeling of Multiphase Mechanically Agitated Reactors, Computational Fluid Dynamics, Hyoung Woo Oh (Ed.), ISBN: 978-953-7619-59-6, InTech, Available from: http://www.intechopen.com/books/computational-fluid-dynamics/computational-flow-modeling-of-multiphase-mechanically-agitated-reactors

INTECH
open science | open minds

InTech Europe
University Campus STeP Ri
Slavka Krautzeka 83/A
51000 Rijeka, Croatia
Phone: +385 (51) 770 447
Fax: +385 (51) 686 166
www.intechopen.com

InTech China
Unit 405, Office Block, Hotel Equatorial Shanghai
No.65, Yan An Road (West), Shanghai, 200040, China
中国上海市延安西路65号上海国际贵都大饭店办公楼405单元
Phone: +86-21-62489820
Fax: +86-21-62489821

IntechOpen